Talanta 247 (2022) 123549

Contents lists available at ScienceDirect

Talanta

journal homepage: www.elsevier.com/locate/talanta

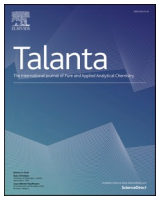

Dextran-coated nanoparticles as immunosensing platforms: Consideration of polyaldehyde density, nanoparticle size and functionality

Shipeng Gao [a], Rebeca M. Torrente-Rodríguez [b], María Pedrero [b], José M. Pingarrón [b], Susana Campuzano [b,**], Javier Rocha-Martin [c,*], José M. Guisán [a,***]

[a] Department of Biocatalysis. Institute of Catalysis and Petrochemistry, ICP/CSIC, Campus UAM, Cantoblanco, 28049, Madrid, Spain
[b] Departamento de Química Analítica, Facultad de CC. Químicas, Universidad Complutense de Madrid, 28040, Madrid, Spain
[c] Department of Biochemistry and Molecular Biology, Faculty of Biology, Complutense University of Madrid, José Antonio Novais 12, Madrid, 28040, Spain

ARTICLE INFO

Keywords:
Iron oxide nanoparticles
Dextran-coated nanoparticles
Antibody orientation
Immunosensors

ABSTRACT

Magnetic nanoparticles (MNPs) can be used as antibody carriers in a wide range of immunosensing applications. The conjugation chemistry for preparing antibody-MNP bionanohybrids should assure the nanoparticle's colloidal dispersity, directional conformation and high biofunctionality retention of attached antibodies. In this work, peroxidase (HRP) was selected as model target analyte, and stable antibody-MNP conjugates were prepared using polyaldehyde-dextrans as multivalent linkers, also to prevent nanoparticles agglomeration and steric shielding of non-specific proteins. Under the manipulation of the oxidation variables, MNP-conjugated antibody showed the highest Fab accessibility, of 1.32 μmol analyte per μmol antibody, corresponding to 139 μmol aldehyde per gram of nanocarrier (5 mM $NaIO_4$, 4 h). Demonstrating anti-interference advantage up to 10% serum, colorimetric immunoassay gave a detection limit (LOD) of 300 ng mL^{-1}, while electrochemical transduction led to a considerable (680 times) improvement, with a LOD of 0.44 ng mL^{-1}. In addition, polyaldehyde-dextran showed priority over polycarboxylated-dextran as the multivalent antibody crosslinker for MNPs in terms of sensitivity and LOD value, while immunosensors constructed with carboxylated magnetic microbeads (HOOC-MBs) outperformed MNPs-based immunoplatforms. This work sheds light on the importance of surface chemistry (type and density of functional groups) and the dimension (nanosize *vs* micrometer) of magnetic carriers to conjugate antibodies with better directional orientation and improve the analytical performance of the resulting immunosensors.

CRediT author statement

Shipeng Gao: Conceptualization, Methodology, Investigation, Writing - original draft, review & editing. **Rebeca M. Torrente-Rodríguez**: Investigation, Writing - review & editing. **María Pedrero**: Supervision, Writing - review & editing, Funding acquisition. **José M. Pingarrón**: Writing - review & editing. **Susana Campuzano**: Conceptualization, Methodology, Supervision, Resources, Writing - review & editing, Funding acquisition. **Javier Rocha-Martin**: Conceptualization, Resources, Writing - review & editing. **José M. Guisán**: Conceptualization, Methodology, Supervision, Resources, Writing - review & editing, Funding acquisition.

1. Introduction

Immunosensors using antibodies as bioreceptors to selectively recognize analytes have garnered tremendous attention from clinical diagnosis to environmental monitoring [1,2]. Nanomaterials are growing as potential biomolecules (such as antibodies, Abs) carriers due to their large surface-to-volume ratio and highly controllable morphology [3]. By just needing a portable magnet, iron oxide magnetic nanoparticles (MNPs) are especially interesting nanocarriers to simplify the washing steps and analytes purification, as opposed to other tedious, time-consuming, and equipment-required options (e.g., centrifugation) [4]. In addition, this directional magnetic-driven virtue ensures the localized enrichment of immunoconjugates onto the working surface of

* Corresponding author.
** Corresponding author.
*** Corresponding author.
E-mail addresses: susanacr@quim.ucm.es (S. Campuzano), javrocha@ucm.es (J. Rocha-Martin), jmguisan@icp.csic.es (J.M. Guisán).

https://doi.org/10.1016/j.talanta.2022.123549
Received 21 March 2022; Received in revised form 10 May 2022; Accepted 12 May 2022
Available online 16 May 2022

screen-printed electrodes by a customized collection tool to perform electrochemical transduction [5]. Accordingly, surface functionalization with dextran, a natural polysaccharide-based neutral polymer, is a useful and well-documented strategy that provides multiple advantages to the nanocarriers [4], including stabilization to avoid self-agglomeration of neighboring nanoparticles [6], antifouling ability against interference proteins [7], and tailored-made surface functionality to immobilize Abs [8]. In addition, despite different dextran derivatives have been developed as multivalent crosslinkers to obtain stable Ab–NPs bioconjugates, including carboxylated- [6], aminated- [9], maleimide activated- [10] and polyaldehyde- [11] dextran, the antibody bioconjugation chemistry should be taken into careful consideration as it directly affects both bioreceptor orientation and functionality [12]. Regardless the transduction technique employed (chemiluminescence, fluorescence, immunochromatography, colorimetry, electrochemical, etc), better immunosensing performance can be expected if the carrier irreversibly binds the Abs well arranged according to the orientation and surface coverage perspectives [13–16].

Primary amines (–NH_2) are appealing candidates for antibody coupling considering their abundant accessible sites to enable high coverage density [17]. However, for the immunoassays using the full-length antibody (immunoglobulin G, IgG), site-directed manipulation of the spatial orientation of antibody-modified NPs, and hence biofunctionality, poses great challenge given the heterogeneous distribution of lysine residues [18]. Efforts have been undertaken to improve the antibody spatial orientation on carriers bearing the NH_2-targeted functionality (glyoxyl groups, epoxy groups and carboxylic groups) [19–21], yet no conjugation chemistry out-performs all others.

Aldehyde moieties, which exhibit advantages over carbodiimide chemistry and ring-open conjugation in terms of simplicity and time-efficiency, can form Schiff bases with NH_2 omitting the pre-activation step [22]. Although glutaraldehyde is a classical aldehyde-bearing linker to attach antibodies on aminated carriers, Abs are subjected to biofunctionality loss after immobilization [23]. The mechanism has been well explained by Gajos et al. [24], showing that glutaraldehyde coupled antibody prefers a "head-on" orientation mainly due to α-NH_2 of *N*-terminus showed much higher reactivity than protonated ε-NH_2 of Lys residues at neutral pH, although the latter has absolute dominance in terms of numbers. Meantime, glyoxyl groups (short aliphatic aldehyde groups) were reported as efficient multivalent ligands to attach Abs within the Lys-rich regions *via* multiple-point interaction [25]. Thus, the relatively larger Lys density on the Fc portion results in the "flat-on" directional conjugation, also favorable to preserve their biological functionality compared to random orientation [19].

Motivated by the promising applications of polyaldehyde chemistry to control the spatial orientation of antibodies coupled to NPs, MNPs with polyaldehyde functionality were chosen as the antibody nanocarriers in this work. The dextran layer, source of polyaldehyde moieties prepared by controllable periodate-induced oxidation, not only acts as a colloidal stabilizer and steric effector of MNPs [7] but also as a multivalent cross-linker to anchor biomolecules on their surface. The supply of numerous NH_2–binding sites, attributed to its long hydrophilic arm, of a high Ab loading capacity [26], a tunable Ab/NP ratio [8] and co-immobilization of specific antibodies against different target analytes [27], were reported using such polyaldehyde dextran nanocarriers, thus demonstrating their promising nanoprobes functionality as well as their multiplexed capabilities. However, to the best of our knowledge, efforts have not been endeavored yet to investigate the effect of polyaldehyde density on the biofunctionality of antibody-carrier.

In this work, we first evaluate the antigen-binding performance (Fab accessibility) of immobilized Abs on polyaldehyde dextran functionalized MNPs with different aldehyde densities. Horseradish peroxidase (HRP) that develops an absorbance or amperometric response upon the presence of the corresponding substrate was selected as model target analyte. Upon the optimal oxidation condition of DexMNPs to maintain antibody-MNPs functionality, the analytical performance of antibody-MNPs immunoplatforms was evaluated and exhaustively compared by means of colorimetric and electrochemical techniques. Finally, the immunosensing performance of antibody carriers with different surface chemistries and particle sizes were electrochemically evaluated.

2. Materials and methods

2.1. Apparatus and electrodes

Colorimetric determination of enzyme activity was made using a Jasco V-730 UV–Visible spectrophotometer (Tsukuba, Japan). Protein concentrations were estimated with a Epoch 2 microplate spectrophotometer (BioTek, Winooski, VT, USA). Amperometric responses were recorded with a CHI1140A (CH Instruments, Austin, TX, USA) potentiostat controlled by the CHI1140A software. Screen-printed carbon electrodes (SPCEs, DRP-110, 4 mm Ø) and DRP-CAC connecting cable were from Metrohm-DropSens S.L. (Oviedo, Spain). A magnetic separator (DynaMag®2) from Invitrogen–Thermo Fisher Scientific was also used.

Other equipment used for NPs characterization include an inductively coupled plasma optical emission spectrometer (ICP-OES, ICP PERKIN ELMER mod. OPTIMA 2100 DV, Waltham, MA, USA), a transmission electron microscope (TEM, JEOL JEM 1010, Peabody, MA, USA), a Zeta Potential Analyzer (Malvern, Zetasizer Nano ZS, Worcestershire, UK), a thermogravimetric analyzer (TA Instruments TGA Q500 Thermobalance, Madrid, Spain), a Bruker IFS66V FTIR Spectrometer (Waltham, MA, USA), and a vibrating sample magnetometer (MagLabVSM, Oxford Instrument, Abingdon, UK). A Jasco V-730 UV–Visible spectrophotometer (Tsukuba, Japan) was also used.

2.2. Reagents

Commercially available carboxylated magnetic microbeads (MBs, 2.8 μm Ø, 10 mg mL^{-1}, Dynabeads M−280, cat. No. 14305D) were purchased from Invitrogen–Thermo Fisher. Iron chloride (III) hexahydrate ($FeCl_3{\cdot}6H_2O$, ≥ 98%), iron chloride (II) tetrahydrate ($FeCl_2{\cdot}4H_2O$, ≥ 99%), ethanol, ammonium hydroxide (NH_4OH, 30%), sodium borohydride ($NaBH_4$), 2,2′-azino-bis (3-ethylbenzo-thiazoline-6-sulfonic acid) (ABTS), nitric acid (HNO_3), sodium bicarbonate ($NaHCO_3$), epichlorohydrin, dextran from *Leuconostoc* spp. (40 kDa), sodium periodate ($NaIO_4$), potassium bromide (KBr), horseradish peroxidase (HRP), anti-horseradish peroxidase antibody (anti-HRP, Catalog Nº. P7899), human serum (from male AB clotted whole blood, Catalog Nº. H6914), hydroquinone (HQ), ethanolamine, *N*-ethyl-*N*′-(3-(dimethylamino)propyl)carbodiimide (EDC), and *N*-hydroxysulfosuccinimide (sulfo-NHS) were obtained from Sigma Aldrich (St. Louis, USA). Hydrogen peroxide (H_2O_2, 30%), sodium hydroxide (NaOH) and potassium iodide (KI) were purchased from PanReac AppliChem (Barcelona, Spain). Sodium chloride (NaCl), potassium chloride (KCl), sodium di-hydrogen phosphate (NaH_2PO_4), di-sodium hydrogen phosphate (Na_2HPO_4), and tris-hydroxymethyl-aminomethane-HCl (Tris–HCl) were brought from Scharlab (Barcelona, Spain). 2-Morpholinoethanesulfonic acid (MES) was purchased from Gerbu. Pierce™ Coomassie Protein Assay Kit (Bradford method, Catalog Nº. 23,200) was purchased from Thermo Fisher Scientific Inc. (Rockford, USA). All other reagents were of analytical grade.

2.3. Synthesis of dextran functionalized MNPs (DexMNPs)

Bare MNPs were prepared by co-precipitation of iron salts in a based solution [28]. Briefly, a volume of 445 mL iron salts solution (0.09 mol Fe^{3+} and 0.054 mol Fe^{2+} in total) was gently added into 75 mL NH_4OH solution (30%) with vigorous magnetic stirring. Change from a clear yellow solution to a black suspension was observed upon the mixture with the alkaline solution. The obtained NPs were further heated up to 90 °C to promote the increment of particle size. After cooling down to

room temperature, the NPs were washed with ethanol and deionized water, successively. Fe concentration of the NPs suspension was determined by ICP-OES, after digesting with HNO_3 at 90 °C for overnight incubation and diluting 1000 times with deionized H_2O.

The dextran coating onto the nanoparticles was performed *via* physical adsorption [29]. To do so, 400 mg dextran was first well dispersed in 2.5 mL NaOH solution (0.5 M) *via* thorough sonication for 5 min. Under vigorous mechanical stirring, 50 mg MNPs dispersed in NaOH solution (1.6 mL, 0.8 M) were added into the above dextran solution drop-by-drop. The mixture solution was continuously stirred for 24 h until a colloidal brown dispersion was obtained.

Although the bare MNPs were aggregated upon the addition to the NaOH solution, a colloidal solution resulted after sufficient coating of dextran layers. The dextran-coated NPs were dialyzed against deionized H_2O for 24 h using a dialysis membrane (12–14 kDa), and then the modified NPs were magnetically collected and resuspended to obtain an homogeneous suspension with a final concentration of 10 mg mL^{-1}.

Further cross-linking treatment was performed to prevent the possible dissociation of dextran layers from NPs surfaces. For this purpose, 1 mL nanoparticle suspension (10 mg mL^{-1}) was mixed with 1 M NaOH, and sonicated for 10 min to get better dispersion. Then, 1.5 mL epichlorohydrin were added into the solution drop-by-drop under vigorous stirring, and the crosslinking was continued for 24 h. After dialysis against deionized H_2O using a dialysis membrane (12–14 kDa), DexMNPs were magnetically recovered and resuspended to obtain an homogeneous suspension with a final concentration of 10 mg mL^{-1}.

2.4. NPs characterization

The morphology and size of the NPs were measured by TEM under 100.0 keV, and the average size and distribution of bare MNPs were calculated using the Image J digital software. The hydrodynamic size of bare MNPs and DexMNPs diluted with deionized H_2O were determined by dynamic light scattering (DLS). The structure and magnetic properties of NPs coated with dextran were characterized using thermogravimetric analysis (TGA), Fourier transform infrared spectroscopy (FTIR) and a vibrating sample magnetometer (VSM). To study the effective adsorption of dextran polysaccharide on the NPs surface, TGA and FTIR measurements were performed with dried samples, prepared by magnetically decanting and drying in an oven for 48 h. To reveal the weight loss after dextran coating, TGA thermograms were measured in the 25–800 °C temperature range under a nitrogen atmosphere at a heating rate of 10 °C min^{-1}. FTIR measurements of dehydrated NPs were recorded within the 4000–400 cm^{-1} wavenumber range after being mixed with KBr and pressed into a pellet (with a NPs to KBr mass ratio of 1:99). The magnetization curves for TGA analysis were obtained at room temperature to investigate the magnetic properties of the samples after applying a field of ±5 T. Briefly, 50 μL of suspension was pipetted into a cotton pellet and dried in an oven for overnight heating before being tightly packed in a holder, and the corresponding magnetization values were normalized to the added total nanoparticles amount.

2.5. Periodate oxidation of DexMNPs and determination of polyaldehyde density

First, 10 mg DexMNPs were magnetically decanted, resuspended into 2 mL periodate solution with different concentrations (2 mM, 5 mM and 10 mM), and sonicated for 1 min to obtain a well-dispersed suspension. The oxidation was carried out under ambient temperature with gentle rotation and protected from light by covering with aluminum foil. After reaction for certain periods (0.5–5 h), DexMNPs were magnetically separated, and the remaining periodate in the supernatant was measured to estimate the aldehyde density [30]. The oxidized NPs suspension (Alde-DexMNPs) was magnetically decanted for 5 min, followed by 5 min of high-speed centrifugation to eliminate the absorbance interference. A mixture of 1 mL saturated $NaHCO_3$ solution and 1 mL KI solution (10%, w/v) was used as reaction solution, and the absorbance at 450 nm was monitored spectrophotometrically upon the addition of 100 μL stock $NaIO_4$ solution or resultant supernatant. The oxidation level of dextran was in equimolar ratio with the consumed amount of periodate after reaction.

2.6. Quantification of the antigen-recognition capacity of the immobilized antibody onto polyaldehyde dextran coated MNPs (Alde-DexMNPs)

Anti-HRP antibodies were bound on the nanocarriers *via* the imide bonds. Unless otherwise stated, all steps involved in the preparation of anti-HRP@MNP bioconjugates were performed at 25 °C under gentle rotation. To do so, a 100 μL aliquot of Alde-DexMNPs suspension was pipetted into a 1.5 mL Eppendorf tube and washed twice with 50 μL $NaHCO_3$ solution (10 mM, pH 10), and 3 min magnetic collection was carried out after each washing step to remove the supernatant. Thereafter, 50 μL of 200 μg mL^{-1} anti-HRP solution (in 10 mM $NaHCO_3$, pH 10) was utilized to suspend the nanocarriers, and the immobilization was performed for 60 min. The bound antibody amount was quantified using the Coomassie Protein Assay Kit. Then, a freshly prepared $NaBH_4$ solution in ice-cold $NaHCO_3$ (10 mM, pH 10) was added to the suspension with 1 mg mL^{-1} final concentration and incubated for 30 min to stabilize the imide bonds. Two washings were performed with phosphate buffer (PB) (10 mM, pH 7.0) to remove unbound antibodies, and the anti-HRP-MNP bioconjugates were resuspended in 50 μL of the same buffer and stored at 4 °C until further use.

To quantify the Fab accessibility of immobilized antibodies, 50 μL anti-HRP-MNP bioconjugates aliquots were incubated with 1 mL of 0.4 mg mL^{-1} HRP (> 20 times saturated concentration) prepared in PB (10 mM, pH 7.0) for 60 min. After the capture of the target analyte, adequate washing steps with PB were performed and HRP-anti-HRP-MNP immunocomplexes were suspended in 20 μL of the same buffered medium for further quantification.

The amount of captured HRP was quantified from the enzymatic activity of HRP-anti-HRP-MNPs immunoconjugates [19]. In brief, 20 μL of the immunocomplex solution were added to 1.96 mL PB (50 mM, pH 6.0) containing 1 mM ABTS (molar extinction coefficient of $ABTS^+$ is 36, 000 M^{-1} cm^{-1}), and 20 μL of H_2O_2 (100 mM) to initiate the real-time absorbance increase that was monitored at 420 nm and 25 °C. One unit of enzyme activity (EA) was defined as the hydrolysis of 1 μmol ABTS per minute by HRP following the parameters stated earlier. Each set of experiments was performed in triplicate to calculate the mean data. The equation of Fab accessibility (capture capacity of immobilized antibodies, equation [1]) is given in the Supporting Information (SI).

2.7. Preparation of immunoassays for colorimetric determination

DexMNPs oxidized under optimal conditions (5 mM IO_4^- for 4 h) were selected as the anti-HRP carriers, and the experimental variables were optimized before carrying out the immunoassays. Conjugation of anti-HRP Abs onto Alde-DexMNPs was performed following the protocol described in Section 2.5.

To carry out the immunoassay, anti-HRP-DexMNPs bioconjugates were incubated in 50 μL of HRP solution (prepared in PB 10 mM, pH 7.0) for 10 min (37 °C with water bath). Next, the HRP-anti-HRP-DexMNPs immunocomplexes were washed twice with 50 μL of PB and resuspended in 20 μL of the same buffer. The colorimetric measurements were recorded following the same protocol as for HRP activity quantification stated in Section 2.5.

2.8. Preparation of immunoassay for electrochemical determination

All steps involved in the preparation of HRP-anti-HRP-MBs and HRP-anti-HRP-MNPs immunoconjugates were performed at 25 °C and 950 rpm, and after each washing-incubation step, 3 min magnetic collection was carried out to remove the supernatant.

2.8.1. Alde-DexMNPs as nanocarriers

A 25 μL-aliquot of the Alde-DexMNPs suspension (10 mg mL^{-1}) was pipetted into a 1.5 mL Eppendorf tube and washed twice with 100 μL of $NaHCO_3$ buffer (10 mM, pH 10). Then, the washed Alde-DexMNPs were resuspended in 100 μL 7.5 μg mL^{-1} anti-HRP solution prepared in 10 mM $NaHCO_3$ buffer, pH 10, and the mixture was incubated for 30 min. Freshly prepared $NaBH_4$ solution (ice-cold 10 mM $NaHCO_3$, pH 10) was added to the anti-HRP-Alde-DexMNPs suspension to obtain an inert surface. After 30 min reduction of residual polyaldehyde groups, the anti-HRP-nanocarriers were washed twice with PB and stored at 4 °C until their use or resuspended in 200 μL PB (10 mM, pH 7.0) to perform the immunoassay.

2.8.2. MBs as microcarriers

3.0 μL-aliquots of the HOOC-MBs suspension were pipetted into 1.5 mL Eppendorf tubes and washed twice with 50 μL of MES buffer (25 mM, pH 5.0) for 10 min. Subsequently, carboxylic groups bearing the MBs were activated by incubating with 25 μL of freshly prepared EDC/Sulfo-NHS mixture solution (50 mg mL^{-1} each) in MES buffer (25 mM, pH 5.0) for 30 min. After two washing steps with MES buffer, activated MBs were incubated for 30 min in 25 μL of 7.5 μg mL^{-1} anti-HRP solution prepared in same buffered medium and after two washings with MES buffer, the remained activated carboxylic groups were blocked with 25 μL of 1 M ethanolamine solution prepared in PB (100 mM, pH 8.0) for 60 min. Next, anti-HRP-MBs were washed once with 50 μL of Tris-HCl (100 mM, pH 7.2) and twice with 50 μL of PBS (100 mM, pH 7.4) and stored in 25 μL PBS at 4 °C until their use.

2.8.3. HOOC-DexMNPs as nanocarriers

Anti-HRP-modified carboxylated nanocarriers were prepared following a similar procedure than that described for MBs but in a one-pot manner. Briefly, a 25 μL-aliquot HOOC-DexMNPs suspension (10 mg mL^{-1}) was pipetted into a 1.5 mL Eppendorf tube and washed twice with 100 μL of MES buffer (25 mM, pH 5.0). As described above, 50 μL of EDC/Sulfo-NHS mixture solution (50 mg mL^{-1}) was used to activate the carboxylic groups, and after twice washing steps with MES buffer, 100 μL of 7.5 μg mL^{-1} anti-HRP solution was incubated for 30 min. Suspension of anti-HRP–HOOC–DexMNPs bioconjugates was treated with the same blocking and triple washing steps as previously described for MBs carriers and resuspended in 200 μL PB (10 mM, pH 7.0).

To perform the immunoassay experiments, the resulting anti-HRP-MBs or 20 μL-aliquot of anti-HRP-DexMNPs (either carboxylic or polyaldehyde functionalized) bioconjugates were incubated with 25 μL HRP solution prepared in PB (10 mM, pH 7.0) for 30 min. Three washing steps with 50 μL of same buffer were carried out to remove the unbound HRP, and HRP-anti-HRP-MBs/DexMNPs were resuspended in 50 μL PB and stored at 4 °C until the amperometric detection was performed.

2.9. Amperometric detection

Despite the antibody carriers, amperometric detection was performed following the same protocol. Briefly, 50 μL of HRP-anti-HRP-MNPs/MBs immunoconjugates were magnetically concentrated onto the surface of the SPCE working electrode, previously inserted in a homemade polymethylmethacrylate (PMMA) casing encapsulating a neodymium magnet. The assembled immunoconjugates/SPCE/casing was immersed into the electrochemical cell containing 1 mM HQ supplemented in 10 mL of PB (50 mM, pH 6.0) and amperometric readings were carried out by applying a constant potential of −200 mV *vs.* the Ag pseudoreference electrode. Upon the stabilization of the background current, 50 μL of freshly prepared H_2O_2 solution (100 mM) in PB were added into the cell to initiate the amperometric detection until the steady state was reached. Triple amperometric measurements were performed to estimate the mean values and their corresponding standard deviation.

3. Results and discussion

3.1. Characterization of dextran-coated iron oxide nanoparticles (DexMNPs)

As DexMNPs were selected as the antibody carriers, a narrow size distribution and good dispersity are crucial parameters for reproducible antibody loading. High-resolution TEM revealed the spherical shape of bare MNPs with an average core size of (14 ± 2) nm (n = 200) (Fig. S1A). Dextran functionalization and epichlorohydrin crosslinking did not alter their morphology (Fig. 1A), but the hydrodynamic size increased to 204 nm with a lower polydispersity index (0.165 *vs.* 0.034), indicating a narrower particle size distribution due to the dextran coating (Fig. 1B).

The efficient dextran functionalization was tested by VSM, TGA and FTIR analysis. VSM tests showed that the NPs exhibit the superparamagnetic behavior at 300 K with no hysteresis (Fig. S1B), and the saturation magnetization of bare NPs decreased from 84 to 46 emu g_{Fe}^{-1} upon the dextran grafting. This reduction confirms the presence of dextran (non-magnetic material), the partial oxidation of magnetite to maghemite in the coating process (accounts for a reduction in saturation magnetization of ~ 10%) and also some surface spin disorder at the nanoparticles magnetic surface [31] (Fig. 1C). The first phase of weight loss (< 200 °C) observed by TGA was attributed to the evaporated water and organic solvent on the MNP surface. The following polymer decomposition and phase transformations caused by the thermal oxidation provoked a further weight decrease [32] (Fig. 1D), resulting in a total 18.7% mass loss. Moreover, the FTIR spectrum revealed the typical Fe–O band of magnetite at 580 cm^{-1} (Fig. S1C) with a small shoulder at 562 cm^{-1}, revealing partial oxidation to maghemite. As well as the characteristic adsorption bands at 3600-3200 cm^{-1} and 1150-1085 cm^{-1} corresponding to O–H and C–O–C stretching of dextran polymer [33], respectively, thus indicating the successful dextran coating of the NPs.

The magnetic separation ability of uncoated MNPs and DexMNPs dispersed in DI H_2O was checked with a handheld magnet (Fig. 1Ea,b). Randomly directed Brownian forces are more decisive than directed magnetic forces for MNPs with a core size smaller than 20 nm [34], so single nanoparticles prone to be inseparable. Upon the applied magnetic field, bare MNPs were hardly recovered from water, while DexMNPs can be easily separated by the external magnet, with a clear supernatant observed after 2 min of magnetic field application. Combining with the enlarged hydrodynamic size from the DLS, the efficient magnetic separation of DexMNPs evidences the presence of small nanoparticle clusters during dextran coating. To probe whether DexMNPs are suitable for the antibody coupling, a buffered solution was utilized to check the stability after dextran coating. The results showed that DexMNPs were well dispersed in alkaline buffer leading to an stable suspension without sediment (Fig. 1Ed), and mild oxidation of dextran backbones maintained its colloidal stability. In contrast, although a homogeneous suspension not prone to sedimentation was visualized with uncoated MNPs when dispersed in DI H_2O, they were aggregated in a short time and fully sedimented at the bottom of the vial (< 60 min) in alkaline medium (Fig. 1Ec). When using a diluted serum solution (containing the HRP target) as the resuspension media, the irreversible adsorption of the protein corona on the MNPs surface was observed after a five-cycle washing treatment, and the typical colorimetric reaction was observed with bare MNPs (ABTS as the substrate of HRP enzymes), while the steric hindrance of the dextran polymers prevented the unspecific adsorption of interference proteins onto the NPs surface (Fig. 1Ee,f).

The ensured colloidal stability under alkaline pH, fast response to a portable magnet and inert surface to steric repelling non-specific proteins make DexMNPs ideal immunocarriers for the preparation of immunosensors.

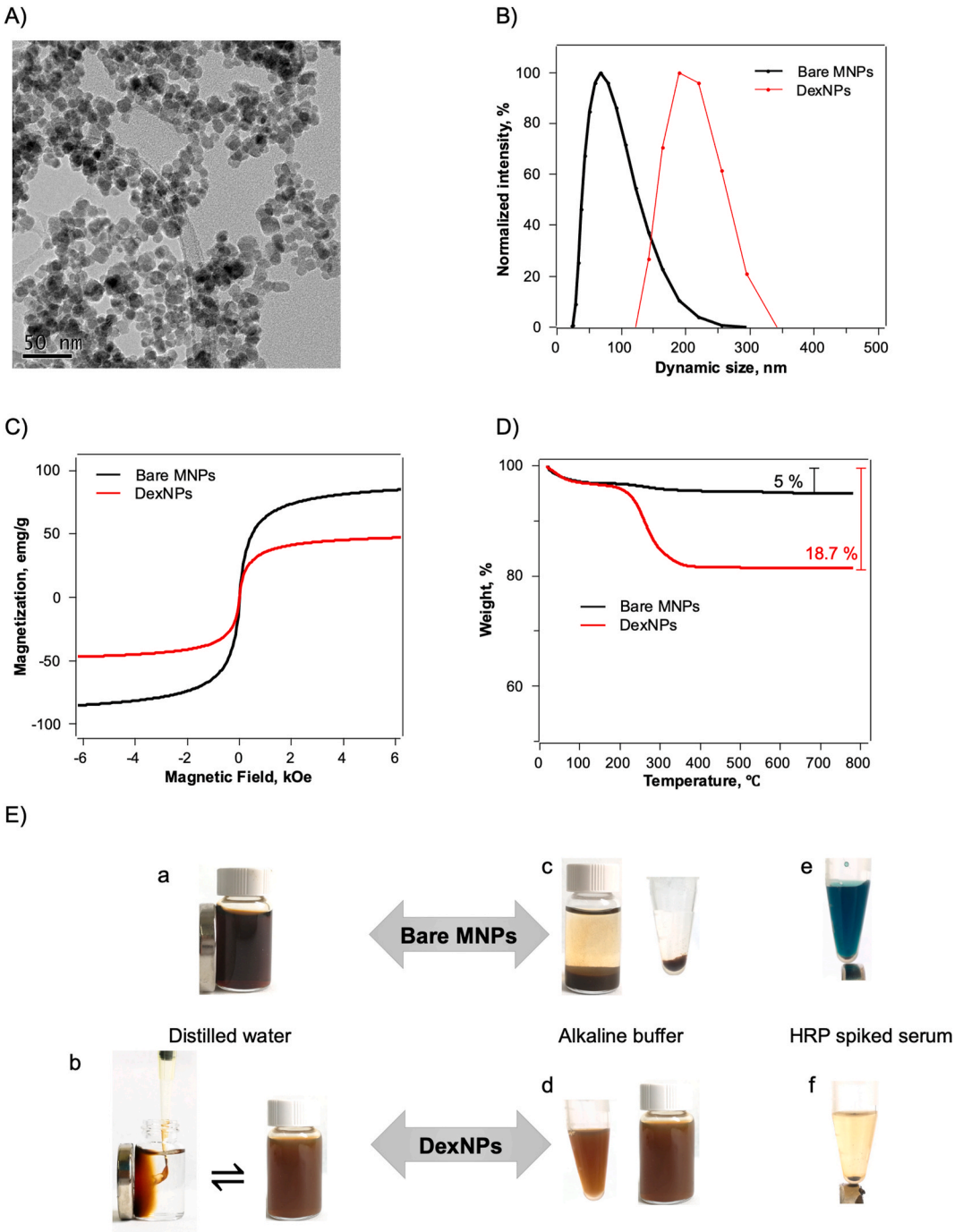

Fig. 1. Structural and morphological characteristics of the nanocarriers. TEM image of the DexMNPs nanoparticles (A). Hydrodynamic size of the bare MNPs and DexMNPs in normalized intensity (B). Saturation magnetization of bare MNPs and DexMNPs using VSM at 300 K (C). Thermogravimetric analysis upon the dextran coating on the bare MNPs (D). Colloidal stability and antifouling characteristics of DexMNPs nanocarriers (E): (a) bare MNPs were a stable suspension in DI H_2O not attracted by a portable magnet, while (c) immediate aggregated and sedimented when exposed into alkaline buffer, and (e) achieved irreversible HRP corona when exposed into the serum (develops blue color after ABTS oxidation); DexMNPs (b) can be magnetically separated facilely and reversible transformed to colloidal status in DI H_2O, and (d) maintain colloidal stability when suspended in alkaline condition, (f) showing dextran polymer steric repulsion to the interaction with nonspecific proteins. (For interpretation of the references to color in this figure legend, the reader is referred to the Web version of this article.)

3.2. Controlled oxidation of dextran polymer to provide polyaldehyde groups

To impart abundant functional groups on DexMNPs as the efficient coupling sites with antibodies, a feasible yet highly controllable methodology is desired. The dextran gentle oxidation (a catalyst-free reaction with high controllability) generating multivalent polyaldehyde groups *via* breaking the vicinal diols between C_3–C_4 or C_3–C_2 suits this requirement (Fig. 2) [35]. The grafted aldehyde functionalities are reactive toward *N*–nucleophiles, among which amine moieties are the most interesting targets for biomolecule immobilization [35]. While the coated dextran layers onto DexMNPs are crucial to providing stability in buffered media (Fig. 1E), strong oxidation conditions may break the dextran chains and cause the dextran layers to be detached from the nanoparticle surface. Therefore, the oxidation degree of the dextran polymer should be carefully regulated.

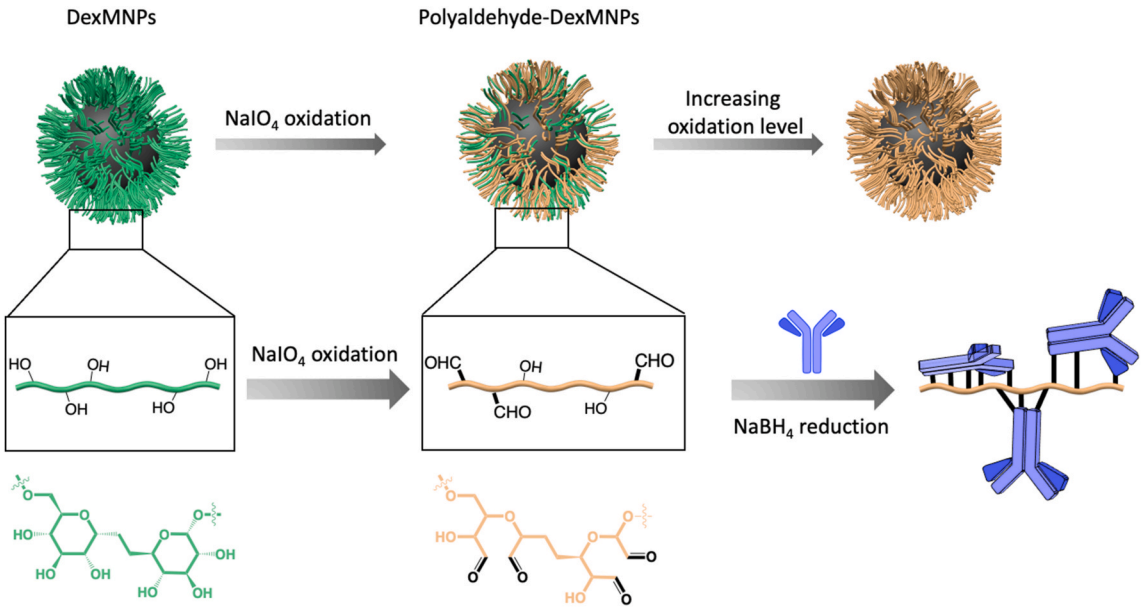

Fig. 2. Schematic illustration of the preparation of polyaldehyde-dextran-modified MNPs as antibody carriers. Intact dextran polymers were marked as green color, while oxidized dextran chains carrying the aldehyde groups were marked as brown color. The generated polyaldehyde dextran will immobilize the antibodies *via* the multiple imide bonds and be reduced to an inert surface after sodium borohydride reduction. (For interpretation of the references to color in this figure legend, the reader is referred to the Web version of this article.)

Two main parameters (periodate concentration and oxidation time) were tested to manage and quantify the aldehyde density onto the NP surface. Fig. S2A shows that, in general, the grafted aldehyde functionalities onto DexMNPs increased with stronger oxidation, with the IO_4^- concentration playing a more dominant role in contributing polyaldehyde density than oxidation time. A medium concentration of IO_4^- (5 mM) for 30 min endows the aldehyde density with 109 μmol g^{-1} nanoparticles which is 1.6-fold larger than that observed with a low IO_4^- concentration (2 mM) for 5 h. A larger IO_4^- concentration (10 mM) provided a higher density of functional groups, as 1 h oxidation yielded 142.6 μmol aldehyde groups g^{-1} nanoparticles, close to the aldehyde density achieved with 5 mM IO_4^- oxidation for 5 h. Moreover, an about 2-fold lower aldehyde density was observed for DexMNPs prepared with 8-times lower dextran coating concentration (Fig. S2B), indicating that the grafted dextran is another important factor determining the aldehyde density on the DexMNPs.

3.3. Immobilization of antibodies onto Alde-DexMNPs nanocarriers and evaluation of their recognition capacity of target analyte

To investigate the influence of the oxidation variables on the nanoparticle-coupled antibody, its surface coverage and the corresponding biofunctionality were evaluated. It is worth mentioning that although the epoxy groups also have reactivity towards NH_2 at alkaline pH, they have much lower reactivity than aldehyde groups [19]. For non-oxidized DexMNPs and using the antibody immobilization protocol described in the "Materials and methods" section, the attachment of antibody *via* epoxy ring-open attacking was negligible.

The effect of polyaldehyde density on the antibody coverage and immobilization rate was studied (Fig. S3). The multipoint aldehyde-Lys interaction promotes the fast coupling of antibodies. Over 18 μg mL^{-1} anti-HRP fully covered the activated carriers in 3 h for high and medium IO_4^- concentrations. Upon observing that immobilization time instead of polyaldehyde density was the decisive factor for antibody coverage, 60 min with ~ 65% surface coverage was selected for the coupling reaction to prevent the steric hindrance caused by the overcrowded antibody.

While a larger IO_4^- concentration promoted a higher anti-HRP coverage (Fig. S4A), the lowest tested IO_4^- concentration yielded about 3-times larger amount of tethered anti-HRP when the longest oxidation time was applied. Medium and high IO_4^- concentrations provided a not too significant increase of bound antibody in the tested oxidation period range (1–5 h).

The biofunctionality capacity of anti-HRP-DexMNPs was further quantified (Fig. S4B). The polyaldehyde density has an apparent impact on the antigen-binding capacity of bound antibodies. When the lowest tested IO_4^- concentration was used, although a growing number of aldehyde groups significantly improved the anti-HRP-DexMNPs recognition capacity (2.3-fold larger), the bound anti-HRP were only able to capture 1.15 μmol HRP per μmol DexMNP-coupled anti-HRP employing 5 h IO_4^- oxidation time. Blocked biofunctionality due to incorrect orientation and limited antibody loading onto nanoparticles (< 40% of density with respect to other IO_4^- concentrations) was obvious for this low IO_4^- concentration, which probably provoked less sensitivity [12, 36]. As can be seen in Fig. S4B, the improvement of the bound anti-HRP biofunctionality with the oxidation time was less measurable for higher IO_4^- concentrations and similar for the other two assayed concentrations. Prolonged oxidation time also caused a gradual reduction of antibody biofunctionality due to their conformation changes and the increased shielding effect of adjacent binding sites [36].

Considering these results, 5 mM IO_4^- and an oxidation time of 4 h were used for further work.

3.4. Optimization of experimental variables and analytical characteristics achieved with the Alde-DexMNPs based immunoassay using colorimetric detection

A direct format immunosensor using the oxidized DexMNPs as the antibody carrier and HRP as the target model analyte was prepared and its analytical characteristics were evaluated. As described in the "Materials and methods" section, the enzyme kinetics calculated by monitoring the absorbance increase during a given period of time was used to quantify the analyte concentration instead of optical density after color development. Therefore, blank samples and samples with an ultralow HRP concentration could not be detected although blue color ($ABTS^+$) maybe developed after long reaction times.

Experimental variables were evaluated in terms of the recognition

rate and HRP binding capacity of anti-HRP@DexMNP immunoconjugates. The incubation temperature did not significantly affect the immunorecognition capacity of the bioconjugates, but when incubation was performed at 37 °C, 98% of the maximum HRP binding was reached in 10 min, while it took about 30 min at 25 °C (Fig. S5A). Antibody coverage was regulated by the immobilization time, with 60 min showing to be adequate to reach the largest binding capacity (Fig. S5B). The concentration of the antibody-coupled nanoparticles showed a significant effect on the binding capacity of the bioconjugates. HRP immobilization up to saturation was obtained with the largest tested concentration (20 mg mL^{-1}) (Fig. S5C). The influence of the buffer composition on the obtained responses showed 5% (v/v) PEG 600 caused a delayed antigen-binding rate due to its high viscosity, while Tween 20 and BSA did not have a negative effect on the immunosensing rate or capacity (Fig. S5D). The densely packed amphiphilic dextran layers provide physical space and steric protection for DexMNPs against non-target proteins, allowing the use of phosphate buffer rather than more complex blocking buffers for immunorecognition.

Under the optimized experimental variables, the calibration plot for the colorimetric anti-HRP@DexMNP-assisted immunoassay (prepared according to the scheme depicted in Fig. 3A) for HRP was constructed. Stock HRP solution was serially diluted to different concentrations until the colorimetric reaction was no longer monitorable. Importantly, DexMNPs (after $NaBH_4$ reduction) without antibody did not show catalytic reaction after the incubation with HRP due to the protective dextran layer. Fig. 3B displays as the enzyme activity (EA) of HRP-anti-HRP@DexMNPs immunoconjugates increased with HRP concentration over the 0.3–7.5 μg mL^{-1} range (R^2 = 0.995), fitting the equation $EA_{immunoconjugates}$ (IU g^{-1}) = (94 ± 3) [HRP] (IU g mL μg $^{-1}$) + (8.1 ± 0.9) (IU g^{-1}). The limit of detection (LOD) for the colorimetric immunoassay was 0.3 μg mL^{-1} since lower HRP concentrations could not be monitored.

A relative standard deviation (RSD) value of 5.8% (n = 3) was calculated for the quantification of 5 μg mL^{-1} HRP. In addition, the accuracy of the results provided by the colorimetric anti-HRP@DexMNPs immunoplatform was evaluated by performing recovery studies with 1 and 10% human serum diluted in PB and spiked with three different HRP concentrations. No matrix effect was observed for the spiked serum samples using both dilution factors. Therefore, the HRP concentrations in the spiked samples were quantified by interpolation of the measurements into the calibration plot constructed in buffered solutions. The average recovery value ranged from 99.1 to 105.8% and from 93.9% to 106.4% for 1 and 10% diluted serum, respectively. In addition, RSD values within the 1.2–10.1% range for the different serum concentrations proved the robustness and acceptable accuracy of the developed colorimetric immunoassay.

3.5. *Optimization of experimental variables and analytical characteristics achieved with the Alde-DexMNPs based immunoplatform using amperometric detection*

Quantification of HRP was additionally performed using electrochemical transduction. As illustrated in Fig. 4A, HRP-anti-HRP@Alde-DexMNPs immunoconjugates were magnetically captured on the working electrode surface of disposable SPCEs and amperometric detection was carried out using the HQ/H_2O_2 system.

Blank signals from anti-HRP@Alde-DexMNPs in the absence of HRP are due to the intrinsic peroxidase-like activity of iron oxide nanoparticles [37], which although undetectable by colorimetric transduction, can be amperometrically detected. In this case, the experimental variables (summarized in Table S1) were selected according to the larger ratio obtained between the amperometric responses obtained in the presence (signal, S) of 100 ng mL^{-1} HRP and in its absence (blank, B), S/B ratio (Fig. S6).

The antibody loading density on the Alde-DexMNPs is a key variable affecting the sensitivity of the assay. Larger S/B ratio was obtained for 7.5 μg mL^{-1} anti-HRP incubated for 30 min (Fig. S6A and B). Moreover, 25 μg Alde-DexMNPs nanocarrier was selected to fabricate the immunoplatforms (Fig. S6C).

Using these mentioned experimental variables, the corresponding HRP calibration plot (Fig. 4B) exhibited a linear response from 1.47 ng mL^{-1} to 30 ng mL^{-1} (R^2 = 0.997), fitting the equation -i, nA = (65 ± 2)

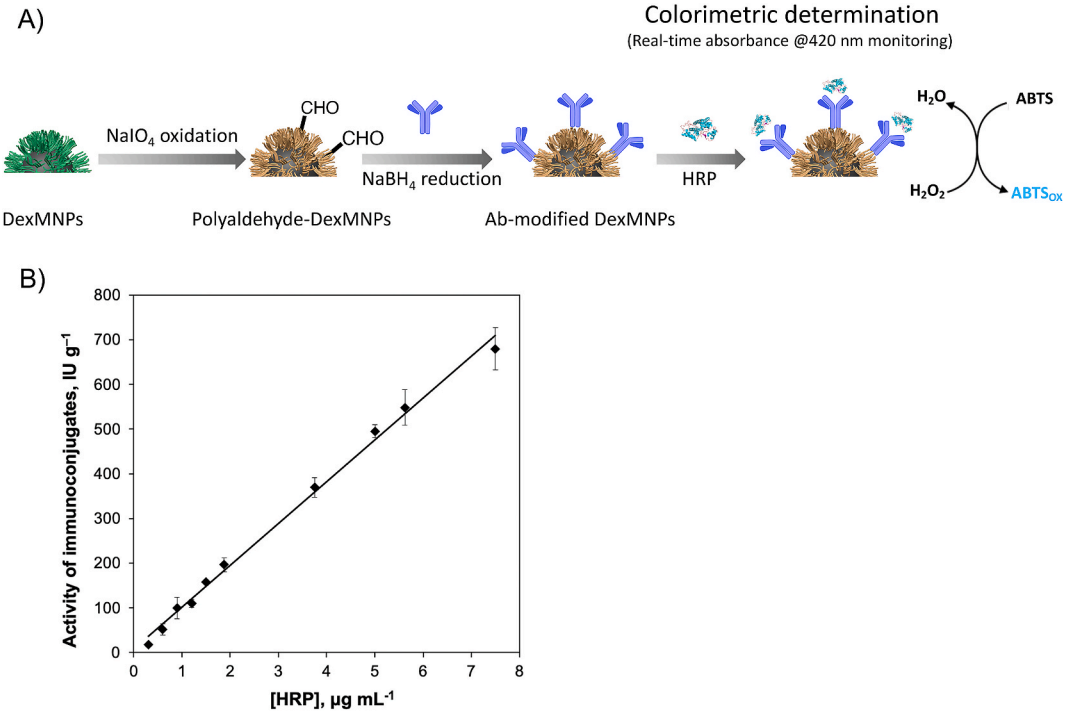

Fig. 3. Schematic illustration of the preparation of Alde-DexMNPs based immunosensors for the colorimetric determination of HRP using ABTS and H_2O_2 as the substrates (A). Calibration plot obtained with the Alde-DexMNPs based immunosensors for the colorimetric analysis of HRP (B).

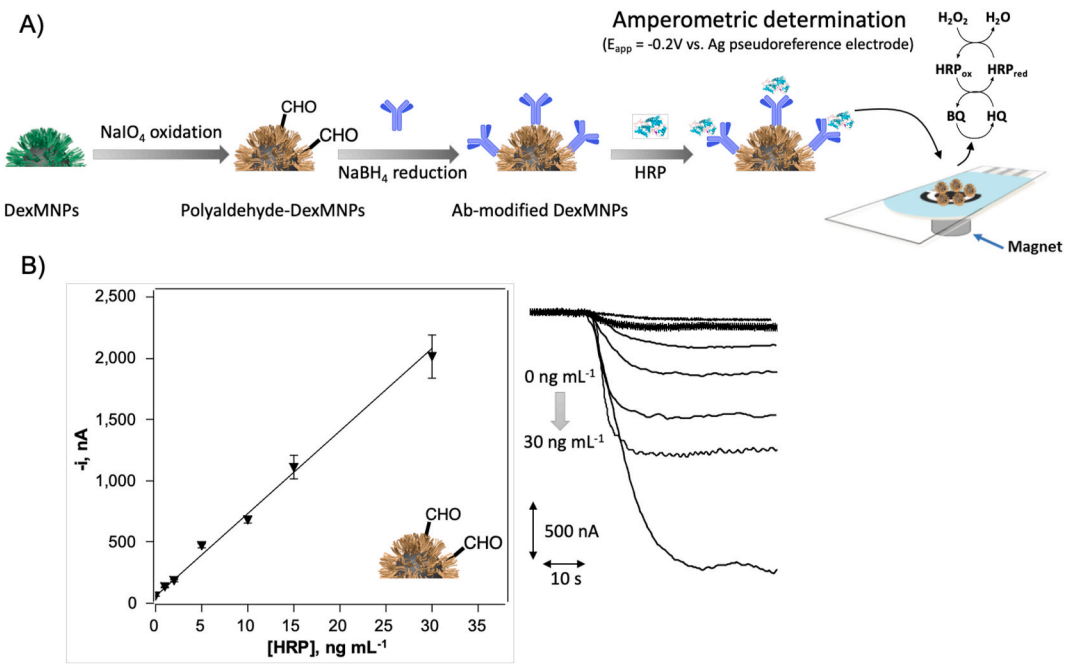

Fig. 4. Schematic illustration of the amperometric determination of HRP using Alde-DexMNPs as the nanocarriers (A). Calibration plot obtained with the Alde-DexMNPs based immunosensors for the amperometric detection of HRP, and display of the amperometric responses of the corresponding HRP concentrations (B).

nA mL^{-1} ng [HRP] + (73 ± 23) nA. LOD and limit of quantification (LOQ) values were 0.44 ng mL^{-1} and 1.47 ng mL^{-1} HRP, calculated according to the 3 × s_b/m and 10 × s_b/m criteria (s_b is the standard deviation of amperometric signals obtained from 10 blank samples, and m is the slope value of the constructed calibration plot), respectively. When the immunosensors were prepared with a 4-fold larger amount of nanocarriers (100 μg instead of 25 μg), a 1.45-fold lower sensitivity (slope values comparison) was obtained, while the linear range extended between 1.95 and 100 ng mL^{-1} (Fig. S7). Importantly, amperometric responses of the HRP-anti-HRP@Alde-DexMNPs immunoconjugates can be measured in the absence of mediator (HQ) (Fig. S8). However, as expected, the presence of HQ significantly enhanced the catalytic process, provoking a 19-times larger sensitivity (44.7 *vs.* 2.3 nA mL^{-1} ng [HRP] slope values of the corresponding calibration plot in the presence and in the absence of HQ).

These results clearly show that electrochemical immunosensing is a more sensitive strategy to determine HRP than the colorimetric one achieving a 680-fold lower LOD value. Nevertheless, the influence of size and surface functionality of the magnetic carriers on the electrochemical response is non-negligible [38,39].

Therefore, we have compared the amperometric measurements obtained with two immunoplatforms differing in the particle size of the antibody carriers. Carboxylated nanoparticles (HOOC-DexMNPs) were derived from Alde-DexMNPs nanoparticles by transforming polyaldehyde groups to carboxyl groups upon imide formation with nitrilotriacetic acid. FTIR confirmed the presence of carboxyl groups after such reaction (Fig. S1C). The behavior of the resulting immunoplatform was compared to that prepared with commercial carboxylated magnetic microbeads (MBs) (2.8 μm in diameter). Both of them can facilely attach anti-HRP *via* carbodiimide-succinimide chemistry.

The analytical characteristics of the carboxylated MNPs/MBs-based immunoplatforms were evaluated after the construction of calibration plots for HRP solutions (Fig. 5A and B). A LOD of 0.78 ng mL^{-1} was calculated using the anti-HRP@HOOC-DexMNPs immunoconjugates according to the 3 × s_b/m criteria. Although a slightly larger LOD was obtained than that achieved with Alde-DexMNPs carriers (0.44 ng mL^{-1}), the use of HOOC-DexMNPs carriers broaded the linear response over the 2.59 ng mL^{-1} to 50 ng mL^{-1} range with an R^2 value of 0.995. An even wider linear range (0.46 ng mL^{-1} to 50 ng mL^{-1}) with a lower LOD (0.14 ng mL^{-1}) were found when HOOC-MBs were employed as the carrier. It reached 2.4 and 1.7 times higher sensitivity (slope values comparison) over carboxylated and polyaldehyde-carrying nanoparticles, respectively. The analytical characteristics of the immunoplatforms fabricated using different antibody carriers (nanoparticles or microparticles) for the amperometric detection of target HRP are summarized in Table 1.

An acceptable reproducibility for intra-day amperometric responses (ten different immunosensing assays) was achieved using the three magnetic particle carriers, yielding RSD values of 8.8 %, 6.6 % and 5.1 % for Alde-DexMNPs, HOOC-DexMNPs and HOOC-MBs, respectively. The storage stability of the fabricated immunoplatforms was evaluated (Fig. S9A, B, C) by measuring the amperometric responses of anti-HRP@carriers (at the nano or micro size), stored at 4 °C in sterilized PB (10 mM, pH 7.0), in the absence and in the presence of HRP (at the concentration indicated in the Figure caption). Antibodies coupled on the three nanoparticle/microparticle carriers showed good stability as no apparent changes in the amperometric responses provided by the resulting immunoplatforms were observed after 26 days of the carriers preparation.

4. Discussion

Comprehensive consideration of the physiochemical properties of nanocarriers (surface chemistry and dimension) is relevant for immunosensing using nanoparticles as the antibody carrier. This, together with antibody immobilization methodology (coverage and orientation), contribute both to the enhanced sensitivity and obtaining reproducible and reliable results [13,38]. A ligand that simultaneously demonstrates the following synergistic advantages is considered as an ideal one for nanocarriers, including providing anchoring sites for the bioreceptors, ensuring antifouling properties against non-specific proteins (specificity), and entitling well dispersity of Ab–NP bioconjugates [40].

Instead of multifunctional ligands composed of several reactive moieties that play distinct roles [41], polyaldehyde dextran fulfills the above requirements to enable bioreceptors with increased flexibility and accessibility toward relevant targets. Moreover, the simple physical

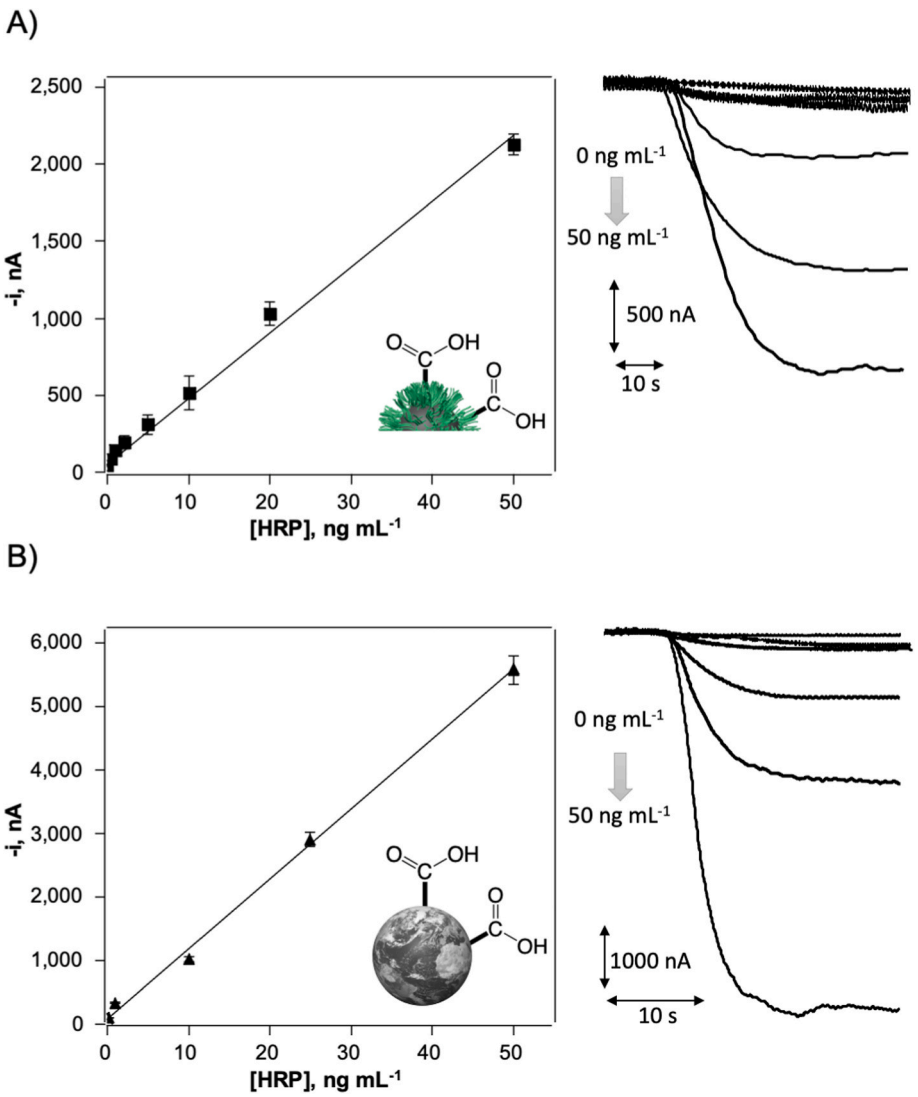

Fig. 5. Calibration plot and amperometric responses obtained with the carboxylated carriers-based immunosensors for the amperometric detection of HRP. Poly-carboxylated nanocarriers (HOOC-DexMNPs) (A) and microparticles carriers (magnetic beads) (B) were used.

Table 1
Analytical characteristics for the amperometric determination of HRP using different magnetic carriers (nanoparticles and microparticles).

Parameters	Antibody carrier			
	Alde-DexMNPs		HOOC-DexMNPs	HOOC-MBs
	25 μg[a]	100 μg[a]		
Linear range, ng mL^{-1}	1.47–30	1.95–100	2.59–50	0.46–50
r	0.997	0.997	0.995	0.998
Slope, nA ng^{-1} mL	65 ± 2	45 ± 1	41 ± 1	110 ± 2
Intercept, nA	73 ± 23	118 ± 61	97 ± 23	94 ± 57
LOD[b], ng mL^{-1}	0.44	0.59	0.78	0.14
LOQ[b], ng mL^{-1}	1.47	1.95	2.59	0.46

[a] The amount of Alde-DexMNPs nanocarriers per sample for the amperometric determination.

[b] LOD and LOQ were estimated by the 3 × s_b/m and 10 × s_b/m criterion, respectively, where m was the slope of the fabricated calibration plot, and s_b was the standard deviation of 10 amperometric responses obtained with the absence of HRP.

coating along with other surface functionalization protocols show cost-effective and less time-consuming advantages [42–44]. The grafted dextran amount has a significant influence on the activated polyaldehyde density (Fig. S2), molecular weight constituting another variable to contribute to different functionality densities and antibody coupling efficiency [6].

In this work, the directional conformation of Alde-DexMNPs-conjugated Abs with high Fab accessibility was explored. Duan et al. [11] revealed that mild oxidation of DexMNPs (5 mM IO_4^- for 6 h) is beneficial to achieve the highest bacteria immunorecognition due to the optimal antibody density, while the oxidation level on the antibody biofunctionality was not discussed. Based on the analysis of antibody coverage and biofunctionality on the Alde-DexMNP nanocarriers, we make a hypothesis about the effect of IO_4^- concentration and poly-aldehyde density on the Fab accessibility of Ab–NPs (Fig. 6). At the considered concentrations, the extension of the oxidation time promotes noticeable higher polyaldehyde density, but does not continuous increase the antibody coverage. It is needed to mention that prolonging the immobilization time not only directly decides the protein anchoring amount, but also favors higher intensity of protein-carrier interaction that is not always advantageous [45]. At low IO_4^- concentration (Fig. 6A), antibody coverage largely depends upon the polyaldehyde density and Ab-nanocarriers density did not reach the saturated monolayer coverage. The multiple interactions occur at this lower Ab coating cause high rigidity and, therefore, denaturation of the immobilized Abs and result in poorer antigen recognition efficiency [36]. As the aldehyde

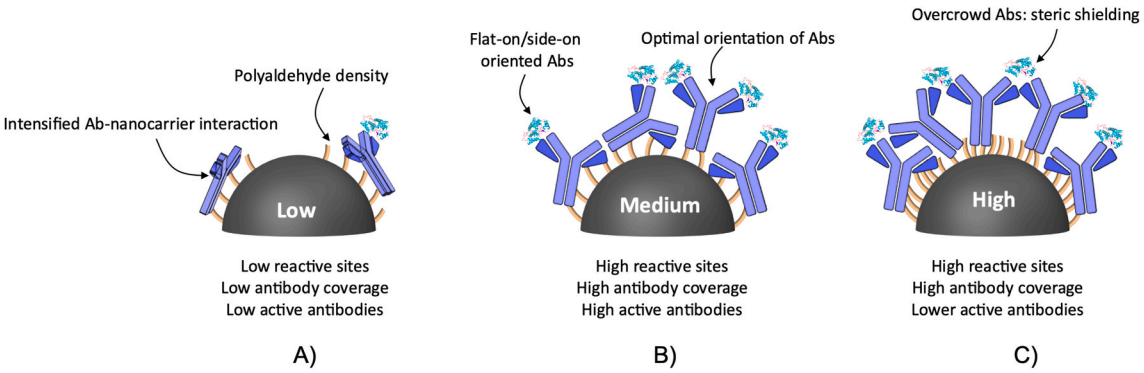

Fig. 6. Illustration of the possible mechanism of antibody orientations on Alde-DexMNP nanocarriers at low (A), medium (B) and high (C) aldehyde densities.

density increases, increasing antibody coverage seems more favored than achieving stronger multiple Ab–NPs interaction, thus weaker covalent linkages are likely to provide a higher degree of Abs motion that contributes to higher Fab accessibility. At medium and high IO_4^- concentration (Fig. 6B and C), aldehyde density is not the limiting factor of Ab coverage after reaching 125 μmol g^{-1} nanocarriers. Significantly improved Ab density would promote the higher proportion of Ab with active (side and flat) orientation [21], thus higher Fab availability until the threshold concentration of monolayer Ab coverage is reached. Further increased Ab density can promote the increase of HRP-Ab-nanocarriers colorimetric signal, while a lower fraction of active Ab may be attributed to the steric shielding of neighboring Abs [36].

Meanwhile, aside from the effect of oxidation degrees on Abs biofunctionality, another concern is the possible dissociation of dextran layers from MNPs surface resulting from harsh oxidation levels, since iron core and polymer shell bonds are formed *via* noncovalent interaction. However, epichlorohydrin crosslinking performed in our study to connect "floating" backbone chains to encage the MNP cores into the polymer-based random coil structure is a well-accepted strategy to reinforce their strong interaction [46]. Due to about 100 times lower IO_4^- concentrations was used for DexMNPs oxidation compared with soluble dextran (2–10 mM *vs* 154–1230 mM) [35], the colloidal stability of Alde-DexMNPs nanocarriers was not obviously affected under the oxidation conditions used in this study (unpublished data), yielding homogeneous and non-aggregated Alde-DexMNP suspension for over 3 months (stored in DI H_2O at 4 °C). Therefore, our optimal oxidation parameters have an unnoticeable deterioration effect concerning DexMNP's stability. On the other hand, Gholipour et al. [47] reported that only a ≈ 1% weight loss of non-crosslinked DexMNPs was caused by a mild oxidation treatment (3.6 mM IO_4^-, 24 h), leading us to believe that our shorter oxidation treatment applied to the strengthened dextran-MNP upon epichlorohydrin crosslinking would not cause considerable polymer detachment. However, intensive oxidation extents are suggested to be avoided.

Being the same aldehyde multivalent linkers, polyaldehyde linkers show larger biofunctionality retention than short glyoxyl linkers [19], due to the better flexibility of anchored Abs grafted by its long spacer, and Abs can stay away from the nanocarrier surface to prevent steric hindrance. It would be interesting to explore the variation of dextran molecular weight in the future to see if Abs would adopt to their suboptimal configuration with excessive longer linker. Further, polycarboxylated dextran was evaluated as an alternative multivalent linker for the coupling reaction. It shares several common characteristics with polyaldehyde dextran crosslinker, including NH_2 targeting, multivalency functionality and strong covalent interaction. Compared with polyaldehyde-dextran, polycarboxylated dextran exhibits higher coupling efficiency with Abs, while suffers lower Ab bioactivity ascribed to the electrostatic repulsion of carboxylic groups against antigens in specific cases [48]. In addition, random conformations upon carbodiimide chemistry render less accessible Fab fragment and < 4% of total Abs maintain active after carbodiimide anchoring [36]. Due to the lower sensitivity and detection limit, polyaldehyde-dextran seems to be more appropriate as the antibody crosslinker in the nanocarriers compared to polycarboxylated-dextran (Figs. 4 and 5A).

Higher sensitivity and lower detection limit using microparticles carriers over nanocarriers were also confirmed, yet there is no general conclusion about the size-related effects of magnetic particles-based immunosensing on analytical performance. The analytical characteristics of the resulting immunosensors can be varied regarding the different carriers (surface chemistry and particle size), analyte sizes and complexity of the matrix solution. Although providing close detection limits, MBs carriers allow a 3.7-fold larger sensitivity than MNPs carriers for soluble AXL immunosensing, while suffering a shorter range of linearity [49]. However, MNPs-based immunosensors have been reported to have better analytical performance than MBs-based immunosensors for histidine-rich protein 2 (HRP2) in terms of detection limit and sensitivity [39], as well as to capture pathogen cells with better sensitivity and recovery efficiency [50,51]. When using nanoparticles as antibody carriers, particle agglomeration, longer magnetic separation time and a possible increased influence of the matrix effect are other main concerns to be taken into account [39,50]. Thus, 100 nm antibody-coupled MNPs were reported to achieve a better selectivity than when using MBs carriers (0.5 μm and 1 μm in diameters) against cells spiked in complicated matrices [51]. In addition, an adequate dilution, yet still within the linear range of the immunosensing assay, allows minimization or even elimination of matrix effects [49]. On the other hand, Alde-DexMNPs are better immunocarriers than carboxylated MBs when considering the operation simplicity, time-saving and cost-effectiveness since nanoparticles are prepared by simple co-precipitation method, have minimal cost, and polyaldehyde chemistry omits prior activation procedure and shortness blocking/stabilization treatment. In addition, nanocarriers can maintain much longer colloidal status and tortuous trajectories to increase the higher possibility to interact with analytes while microparticles tend to sediment due to gravity attraction even under continuous stirring.

The characteristic of the immunosensing protocols reported in this work have been compared with other immunosensors reported so far for the determination of HRP (Table S2). Directional oriented antibody *via* Fc-binding domain contributed to a 10-fold higher sensitivity than that obtained through adsorption interaction reaching a LOD of 0.1 ng mL^{-1} HRP, while tedious surface functionalization of the microtiter plate is necessary [16]. The change of colorimetric reader (absorbance intensity) from a spectrophotometer to a portable smartphone camera also results in good LOD [52], but purification of analytes is not facile for microplates. Microfluidic paper-based devices can give straightforward visible results within a short time providing high portability and simplicity, although power-free fluid transport limits the sensitivity

[53]. Similarly, lateral flow immunoassay revealed over 3 orders of detection linearity, while the detection limit was obviously lower than that achieved with other fabricated immunoplatforms even with chemiluminescence signal amplification [54]. Recently, novel quantification techniques have further improved the detection limit to a great extent, including electrochemical [12] and surface-enhanced Raman scattering (SERS) [55], showing the importance of analytical methods.

5. Conclusion

Exploring novel NH_2-directed conjugation with antibodies, which is convenient, efficient and cost-effective, and also has better control over the reaction sites, is a highlighted common interest for immunosensing applications. In this study, versatile Alde-DexMNPs have been proven as promising "ideal" antibody nanocarriers, the assembled Ab–MNPs bioconjugates showing good robustness, sensitivity and selectivity toward HRP analyte upon the evaluation of four different variables on the immunosensing performance. Better directional conformation and high Fab accessibility of coupled antibodies were obtained *via* the tunable regulation of polyaldehyde density on the nanocarriers surface, and the constructed immunosensors exhibited satisfying analytes recovery from 10% diluted serum with colorimetric immunoassay, while the amperometric assay (HQ/H_2O_2 system) significantly improved 670 times the LOD. Despite carboxylated MBs outperform the nanocarriers and show lower detection limit and wider linearity, still nanocarriers may be considered as an interesting alternative to microparticles in terms of cost-effectiveness and simplicity. Further, our homemade DexMNP nanocarrier is easily transferable as suitable support for the interrogation of other biomacromolecules based on distinct configuration formats, therefore holding a great application prospect in both colorimetric and electrochemical immunoassays.

Declaration of competing interest

The authors declare that they have no known competing financial interests or personal relationships that could have appeared to influence the work reported in this paper.

Acknowledgments

We acknowledge financial support from Madrid regional government (Doctorados Industriales en la Comunidad de Madrid, IND2018/BIO-9480). The financial support of PID2019-103899RB-I00 (Spanish Ministerio de Ciencia e Innovación) Research Project and the TRANSNANOAVANSENS-CM Program from the Comunidad de Madrid (Grant S2018/NMT-4349) are gratefully acknowledged. The group of MAMBIO from the Institute of Materials Science in Madrid (ICMM/CSIC) is acknowledged by providing the magnetic nanoparticles and protocols for dextran coating. Shipeng Gao also acknowledges the financial support from the China Scholarship Council (201808440415).

Appendix A. Supplementary data

Supplementary data to this article can be found online at https://doi.org/10.1016/j.talanta.2022.123549.

References

[1] S. Campuzano, R. Barderas, P. Yáñez-Sedeño, J.M. Pingarron, Electrochemical biosensing to assist multiomics analysis in precision medicine, Curr. Opin. Electrochem. 28 (2021) 100703, https://doi.org/10.1016/j.coelec.2021.100703.
[2] R. Chen, Y. Dong, F. Hong, X. Zhang, X. Wang, J. Wang, Y. Chen, Polydopamine nanoparticle-mediated, click chemistry triggered, microparticle-counting immunosensor for the sensitive detection of ochratoxin A, J. Hazard Mater. 428 (2022) 128206, https://doi.org/10.1016/j.jhazmat.2021.128206.
[3] S. Mallick, K.R.B. Singh, V. Nayak, J. Singh, R.P. Singh, Potentialities of core@shell nanomaterials for biosensor technologies, Mater. Lett. 306 (2022) 130912, https://doi.org/10.1016/j.matlet.2021.130912.
[4] C. Tassa, S.Y. Shaw, R. Weissleder, Dextran-coated iron oxide nanoparticles: a versatile platform for targeted molecular imaging, molecular diagnostics, and therapy, Acc. Chem. Res. 44 (10) (2011) 842–852, https://doi.org/10.1021/ar200084x.
[5] M. Blazquez-Garcia, B. Arevalo, V. Serafin, S. Benede, L. Mata, P. Galan-Malo, I. Segura-Gil, M.D. Perez, J.M. Pingarron, S. Campuzano, Ultrasensitive detection of soy traces by immunosensing of glycinin and beta-conglycinin at disposable electrochemical platforms, Talanta 241 (2022) 123226, https://doi.org/10.1016/j.talanta.2022.123226.
[6] F. Kunc, C.J. Moore, R.E. Sully, A.J. Hall, V. Gubala, Polycarboxylated dextran as a multivalent linker: synthesis and target recognition of the antibody-nanoparticle bioconjugates in PBS and serum, Langmuir 35 (14) (2019) 4909–4917, https://doi.org/10.1021/acs.langmuir.8b03833.
[7] C.J. Moore, H. Monton, R. O'Kennedy, D.E. Williams, C. Nogues, C. Crean Nee Lynam, V. Gubala, Controlling colloidal stability of silica nanoparticles during bioconjugation reactions with proteins and improving their longer-term stability, handling and storage, J. Mater. Chem. B 3 (10) (2015) 2043–2055, https://doi.org/10.1039/c4tb01915f.
[8] M. Gharaat, R.H. Sajedi, M. Shanehsaz, N. Jalilian, M. Mirshahi, M. Gholamzad, A dextran mediated multicolor immunochromatographic rapid test strip for visual and instrumental simultaneous detection of Vibrio cholera O1 (Ogawa) and Clostridium botulinum toxin A, Microchim. Acta 184 (12) (2017) 4817–4825, https://doi.org/10.1007/s00604-017-2527-2.
[9] K. Rees, M.V. Tran, M. Massey, H. Kim, K.D. Krause, W.R. Algar, Dextran-functionalized semiconductor quantum dot bioconjugates for bioanalysis and imaging, Bioconjugate Chem. 31 (3) (2020) 861–874, https://doi.org/10.1021/acs.bioconjchem.0c00019.
[10] N. Ding, K. Sano, K. Kanazaki, M. Ohashi, J. Deguchi, Y. Kanada, M. Ono, H. Saji, In vivo HER2-targeted magnetic resonance tumor imaging using iron oxide nanoparticles conjugated with anti-HER2 fragment antibody, Mol. Imag. Biol. 18 (6) (2016) 870–876, https://doi.org/10.1007/s11307-016-0977-2.
[11] H.L. Duan, Z.Q. Shen, X.W. Wang, F.H. Chao, J.W. Li, Preparation of immunomagnetic iron-dextran nanoparticles and application in rapid isolation of E.coli O157:H7 from foods, World J. Gastroenterol. 11 (24) (2005) 3660–3664, https://doi.org/10.3748/wjg.v11.i24.3660.
[12] M. Sharafeldin, K. McCaffrey, J.F. Rusling, Influence of antibody immobilization strategy on carbon electrode immunoarrays, Analyst 144 (17) (2019) 5108–5116, https://doi.org/10.1039/C9AN01093A.
[13] B. Saha, P. Songe, T.H. Evers, M.W.J. Prins, The influence of covalent immobilization conditions on antibody accessibility on nanoparticles, Analyst 142 (22) (2017) 4247–4256, https://doi.org/10.1039/c7an01424d.
[14] J. Hu, S. Zhou, L. Zeng, Q. Chen, H. Duan, X. Chen, X. Li, Y. Xiong, Hydrazide mediated oriented coupling of antibodies on quantum dot beads for enhancing detection performance of immunochromatographic assay, Talanta 223 (Part 1) (2021) 121723, https://doi.org/10.1016/j.talanta.2020.121723.
[15] B.-Y. Liao, C.-J. Chang, C.-F. Wang, C.-H. Lu, J.-K. Chen, Controlled antibody orientation on Fe_3O_4 nanoparticles and CdTe quantum dots enhanced sensitivity of a sandwich-structured electrogenerated chemiluminescence immunosensor for the determination of human serum albumin, Sensor. Actuator. B Chem. 336 (2021) 129710, https://doi.org/10.1016/j.snb.2021.129710.
[16] H.M. Yang, S.J. Liang, J.B. Tang, Y. Chen, Y.Z. Cheng, Immobilization of unraveled immunoglobulin G using well-oriented ZZ-His protein on functionalized microtiter plate for sensitive immunoassay, Anal. Biochem. 432 (2) (2013) 134–138, https://doi.org/10.1016/j.ab.2012.09.028.
[17] N.G. Welch, J.A. Scoble, B.W. Muir, P.J. Pigram, Orientation and characterization of immobilized antibodies for improved immunoassays (Review), Biointerphases 12 (2) (2017), 02D301, https://doi.org/10.1116/1.4978435.
[18] S. Gao, J.M. Guisan, J. Rocha-Martin, Oriented immobilization of antibodies onto sensing platforms - a critical review, Anal. Chim. Acta 1189 (2022) 338907, https://doi.org/10.1016/j.aca.2021.338907.
[19] S. Gao, F. Rojas-Vega, J. Rocha-Martin, J.M. Guisan, Oriented immobilization of antibodies through different surface regions containing amino groups: selective immobilization through the bottom of the Fc region, Int. J. Biol. Macromol. 177 (2021) 19–28, https://doi.org/10.1016/j.ijbiomac.2021.02.103.
[20] P. Batalla, J.M. Bolivar, F. Lopez-Gallego, J.M. Guisan, Oriented covalent immobilization of antibodies onto heterofunctional agarose supports: a highly efficient immuno-affinity chromatography platform, J. Chromatogr. A 1262 (2012) 56–63, https://doi.org/10.1016/j.chroma.2012.08.058.
[21] D. Lou, L. Ji, L. Fan, Y. Ji, N. Gu, Y. Zhang, Antibody-oriented strategy and mechanism for the preparation of fluorescent nanoprobes for fast and sensitive immunodetection, Langmuir 35 (14) (2019) 4860–4867, https://doi.org/10.1021/acs.langmuir.9b00150.
[22] W.G. Morais Junior, T.F. Pacheco, S. Gao, P.A. Martins, J.M. Guisán, N.S. Caetano, Sugarcane bagasse saccharification by enzymatic hydrolysis using endocellulase and β-glucosidase immobilized on different supports, Catalysts 11 (3) (2021) 340, https://doi.org/10.3390/catal11030340.
[23] M. Fuentes, C. Mateo, J.M. Guisan, R. Fernandez-Lafuente, Preparation of inert magnetic nano-particles for the directed immobilization of antibodies, Biosens. Bioelectron. 20 (7) (2005) 1380–1387, https://doi.org/10.1016/j.bios.2004.06.004.
[24] K. Gajos, K. Szafraniec, P. Petrou, A. Budkowski, Surface density dependent orientation and immunological recognition of antibody on silicon: TOF-SIMS and surface analysis of two covalent immobilization methods, Appl. Surf. Sci. 518 (2020) 146269, https://doi.org/10.1016/j.apsusc.2020.146269.
[25] P. Batalla, C. Mateo, V. Grazu, R. Fernandez-Lafuente, J.M. Guisan, Immobilization of antibodies through the surface regions having the highest density in lysine

groups on finally inert support surfaces, Process Biochem. 44 (3) (2009) 365–368, https://doi.org/10.1016/j.procbio.2008.11.017.
[26] C.J. Moore, G. Giovannini, F. Kunc, A.J. Hall, V. Gubala, 'Overloading' fluorescent silica nanoparticles with dyes to improve biosensor performance, J. Mater. Chem. B 5 (28) (2017) 5564–5572, https://doi.org/10.1039/c7tb01284e.
[27] S.Y. Yang, Z.F. Jian, H.E. Horng, C.-Y. Hong, H.C. Yang, C.C. Wu, Y.H. Lee, Dual immobilization and magnetic manipulation of magnetic nanoparticles, J. Magn. Magn Mater. 320 (21) (2008) 2688–2691, https://doi.org/10.1016/j.jmmm.2008.05.048.
[28] R. Massart, Preparation of aqueous magnetic liquids in alkaline and acidic media, IEEE Trans. Magn. 17 (2) (1981) 1247–1248, https://doi.org/10.1109/tmag.1981.1061188.
[29] M. Carmen Bautista, O. Bomati-Miguel, M. del Puerto Morales, C.J. Serna, S. Veintemillas-Verdaguer, Surface characterisation of dextran-coated iron oxide nanoparticles prepared by laser pyrolysis and coprecipitation, J. Magn. Magn Mater. 293 (1) (2005) 20–27, https://doi.org/10.1016/j.jmmm.2005.01.038.
[30] C. Mateo, G. Fernandez-Lorente, J. Rocha-Martin, J.M. Bolivar, J.M. Guisan, Oriented covalent immobilization of enzymes on heterofunctional-glyoxyl supports, in: J.M. Guisan (Ed.), Immobilization of Enzymes and Cells, Humana Press, Totowa, NJ, 2013, pp. 73–88, https://doi.org/10.1007/978-1-62703-550-7_6.
[31] D.K. Mondal, S. Jonak, N. Paul, J.P. Borah, Dextran mediated $MnFe_2O_4$/ZnS magnetic fluorescence nanocomposites for controlled self-heating properties, RSC Adv. 11 (21) (2021) 12507–12519, https://doi.org/10.1039/d0ra09745d.
[32] H.K. Can, S. Kavlak, S. ParviziKhosroshahi, A. Guner, Preparation, characterization and dynamical mechanical properties of dextran-coated iron oxide nanoparticles (DIONPs), Artif. Cells Nanomed, Biotechnol. 46 (2) (2018) 421–431, https://doi.org/10.1080/21691401.2017.1315428.
[33] M. Peng, H. Li, Z. Luo, J. Kong, Y. Wan, L. Zheng, Q. Zhang, H. Niu, A. Vermorken, W. Van de Ven, C. Chen, X. Zhang, F. Li, L. Guo, Y. Cui, Dextran-coated superparamagnetic nanoparticles as potential cancer drug carriers in vivo, Nanoscale 7 (25) (2015) 11155–11162, https://doi.org/10.1039/c5nr01382h.
[34] C.T. Yavuz, J.T. Mayo, W.W. Yu, A. Prakash, J.C. Falkner, S. Yean, L. Cong, H. J. Shipley, A. Kan, M. Tomson, D. Natelson, V.L. Colvin, Low-field magnetic separation of monodisperse Fe_3O_4 nanocrystals, Science 314 (5801) (2006) 964–967, https://doi.org/10.1126/science.1131475.
[35] J. Maia, R.A. Carvalho, J.F.J. Coelho, P.N. Simões, M.H. Gil, Insight on the periodate oxidation of dextran and its structural vicissitudes, Polymer 52 (2) (2011) 258–265, https://doi.org/10.1016/j.polymer.2010.11.058.
[36] B. Saha, T.H. Evers, M.W. Prins, How antibody surface coverage on nanoparticles determines the activity and kinetics of antigen capturing for biosensing, Anal. Chem. 86 (16) (2014) 8158–8166, https://doi.org/10.1021/ac501536z.
[37] P.C. Naha, Y. Liu, G. Hwang, Y. Huang, S. Gubara, V. Jonnakuti, A. Simon-Soro, D. Kim, L. Gao, H. Koo, D.P. Cormode, Dextran-coated iron oxide nanoparticles as biomimetic catalysts for localized and pH-activated biofilm disruption, ACS Nano 13 (5) (2019) 4960–4971, https://doi.org/10.1021/acsnano.8b08702.
[38] S.-I. Tu, S. Reed, A. Gehring, Y. He, G. Paoli, Capture of Escherichia coli O157:H7 using immunomagnetic beads of different size and antibody conjugating chemistry, Sensors 9 (2) (2009) 717–730, https://doi.org/10.3390/s90200717.
[39] S. Castilho Mde, T. Laube, H. Yamanaka, S. Alegret, M.I. Pividori, Magneto immunoassays for Plasmodium falciparum histidine-rich protein 2 related to malaria based on magnetic nanoparticles, Anal. Chem. 83 (14) (2011) 5570–5577, https://doi.org/10.1021/ac200573s.
[40] M. Tasso, M.K. Singh, E. Giovanelli, A. Fragola, V. Loriette, M. Regairaz, F. Dautry, F. Treussart, Z. Lenkei, N. Lequeux, T. Pons, Oriented bioconjugation of unmodified antibodies to quantum dots capped with copolymeric ligands as versatile cellular imaging tools, ACS Appl. Mater. Interfaces 7 (48) (2015) 26904–26913, https://doi.org/10.1021/acsami.5b09777.
[41] V. Mangini, V. Maggi, A. Trianni, F. Melle, E. De Luca, A. Pennetta, R. Del Sole, G. Ventura, T.R.I. Cataldi, R. Fiammengo, Directional immobilization of proteins on gold nanoparticles is essential for their biological activity: leptin as a case study, Bioconjugate Chem. 31 (1) (2020) 74–81, https://doi.org/10.1021/acs.bioconjchem.9b00748.
[42] C.S. Ciobanu, S.L. Iconaru, E. Gyorgy, M. Radu, M. Costache, A. Dinischiotu, P. Le Coustumer, K. Lafdi, D. Predoi, Biomedical properties and preparation of iron oxide-dextran nanostructures by MAPLE technique, Chem. Cent. J. 6 (1) (2012) 17, https://doi.org/10.1186/1752-153X-6-17.
[43] G. Predoi, C.S. Ciobanu, S.L. Iconaru, D. Predoi, D.B. Dreghici, A. Groza, F. Barbuceanu, C. Cimpeanu, M.L. Badea, S.F. Barbuceanu, C.F. Furnaris, C. Belu, L. Ghegoiu, M.S. Raita, Preparation and characterization of dextran coated iron oxide nanoparticles thin layers, Polymers 13 (14) (2021) 2351, https://doi.org/10.3390/polym13142351.
[44] S.L. Iconaru, S.A. Predoi, M. Beuran, C.S. Ciobanu, R. Trusca, R. Ghita, I. Negoi, G. Teleanu, S.C. Turculet, M. Matei, M. Badea, A.M. Prodan, Fabrication and characterization of iron oxide dextran composite layers, AIP Conf. Proc. (1) (1932), 030019, https://doi.org/10.1063/1.5024169, 2018.
[45] R.C. Rodrigues, A. Berenguer-Murcia, D. Carballares, R. Morellon-Sterling, R. Fernandez-Lafuente, Stabilization of enzymes via immobilization: multipoint covalent attachment and other stabilization strategies, Biotechnol. Adv. 52 (2021) 107821, https://doi.org/10.1016/j.biotechadv.2021.107821.
[46] H. Arami, A. Khandhar, D. Liggitt, K.M. Krishnan, In vivo delivery, pharmacokinetics, biodistribution and toxicity of iron oxide nanoparticles, Chem. Soc. Rev. 44 (23) (2015) 8576–8607, https://doi.org/10.1039/c5cs00541h.
[47] N. Gholipour, M. Akhlaghi, A. Mokhtari Kheirabadi, P. Geramifar, D. Beiki, Development of Ga-68 labeled, biotinylated thiosemicarbazone dextran-coated iron oxide nanoparticles as multimodal PET/MRI probe, Int. J. Biol. Macromol. 148 (2020) 932–941, https://doi.org/10.1016/j.ijbiomac.2020.01.208.
[48] A.W. Drake, M.L. Tang, G.A. Papalia, G. Landes, M. Haak-Frendscho, S.L. Klakamp, Biacore surface matrix effects on the binding kinetics and affinity of an antigen/antibody complex, Anal. Biochem. 429 (1) (2012) 58–69, https://doi.org/10.1016/j.ab.2012.06.024.
[49] V. Serafín, R.M. Torrente-Rodríguez, M. Batlle, P. García de Frutos, S. Campuzano, P. Yáñez-Sedeño, J.M. Pingarron, Comparative evaluation of the performance of electrochemical immunosensors using magnetic microparticles and nanoparticles. Application to the determination of tyrosine kinase receptor AXL, Microchim. Acta 184 (11) (2017) 4251–4258, https://doi.org/10.1007/s00604-017-2455-1.
[50] D. Brandao, S. Liebana, S. Campoy, S. Alegret, M. Isabel Pividori, Immunomagnetic separation of Salmonella with tailored magnetic micro and nanocarriers. A comparative study, Talanta 143 (2015) 198–204, https://doi.org/10.1016/j.talanta.2015.05.035.
[51] J. Chen, B. Park, Effect of immunomagnetic bead size on recovery of foodborne pathogenic bacteria, Int. J. Food Microbiol. 267 (2018) 1–8, https://doi.org/10.1016/j.ijfoodmicro.2017.11.022.
[52] S.K. Vashist, T. van Oordt, E.M. Schneider, R. Zengerle, F. von Stetten, J.H. Luong, A smartphone-based colorimetric reader for bioanalytical applications using the screen-based bottom illumination provided by gadgets, Biosens. Bioelectron. 67 (2015) 248–255, https://doi.org/10.1016/j.bios.2014.08.027.
[53] L.S.A. Busa, M. Maeki, A. Ishida, H. Tani, M. Tokeshi, Simple and sensitive colorimetric assay system for horseradish peroxidase using microfluidic paper-based devices, Sensor. Actuator. B Chem. 236 (2016) 433–441, https://doi.org/10.1016/j.snb.2016.06.013.
[54] B.G. An, H.R. Kim, M.J. Kang, J.G. Park, Y.W. Chang, J.C. Pyun, Chemiluminescent lateral-flow immunoassays by using in-situ synthesis of CdS NW photosensor, Anal. Chim. Acta 927 (2016) 99–106, https://doi.org/10.1016/j.aca.2016.04.048.
[55] M.J. Oliveira, I. Cunha, M.P. de Almeida, T. Calmeiro, E. Fortunato, R. Martins, L. Pereira, H.J. Byrne, E. Pereira, H. Aguas, R. Franco, Reusable and highly sensitive SERS immunoassay utilizing gold nanostars and a cellulose hydrogel-based platform, J. Mater. Chem. B 9 (36) (2021) 7516–7529, https://doi.org/10.1039/D1TB01404H.